Research Article | Vol. 10, No. 3 / 1 March 2020 / Optical Materials Express 818
Optical Materials EXPRESS

Inkjet-printed lasing silk text on reusable distributed feedback boards

MUHAMMD UMAR,[1,5] WENYI LI,[2,5] GIORGIO E. BONACCHINI,[2,5] KYUNGTAEK MIN,[3] SARA ARIF,[1] FIORENZO G. OMENETTO,[2,6] AND SUNGHWAN KIM[1,4,7]

[1]*Department of Energy Systems Research, Ajou University, Suwon 16499, South Korea*
[2]*Department of Biomedical Engineering, Tufts University, Medford, MA 02155, USA*
[3]*Department of Nano-Optical Engineering, Korea Polytechnic University, Siheung 15073, South Korea*
[4]*Department of Physics, Ajou University, Suwon 16499, South Korea*
[5]*These authors contributed equally to this work.*
[6]*fiorenzo.omenetto@tufts.edu*
[7]*sunghwankim@ajou.ac.kr*

Abstract: Inkjet printing is an attractive bottom-up microfabrication technology owing to its simplicity, ease of use, and low cost. This method is particularly suitable for patterning of biomaterials because biofunctionality and bioactivity can be preserved during the patterning process in the absence of harsh conditions such as heat, UV radiation, and plasma. However, it is still challenging to apply this technology to biomaterial-based soft photonics, which requires precise control over morphology and uniformity to confine photons efficiently. This study introduces inkjet printing to create silk protein patterns to emit/guide a single-mode distributed feedback (DFB) laser on a single platform. A thin TiO_2 coated grating enables coherent feedback of the generated photons for any shape of the printed silk pattern. The lasing wavelength can be adjusted by adding gold nanoparticles to the silk/dye ink. Photonic components of lasers and waveguides are drawn on a DFB board, and the lasing light can be extracted through adjacent waveguides. The printed components can be reformed by post modification (water-removal and reprinting). Additionally, optically absorptive melanin nanoparticles placed on the waveguide can attenuate the propagating light, thus adding utility for sensing applications. This allows a new method to fabricate cost-effective, easily functionalized, and versatile biomaterial photonic chips for advanced sensing and diagnosis.

1. Introduction

Material patterning is important for demonstrating micro/nanophotonic components and for generating and manipulating photons in displays [1–5], biosensors [6–9], and data processing [10–14] applications. Conventional fabrication methods, including photolithography [15–17], vacuum deposition [18–20], and etching [21–23], have been used to build precise and reliable photonic devices. However, these techniques may not be suitable for patterning soft biomaterials because the material traits and biofunctionalities could be influenced by exposure to UV light, vacuum, and plasma. Recently, printing technology has moved beyond texts and graphics into photonics because it is a direct, cost-effective, maskless, additive, and eco-friendly method to obtain photonic components. Among the many available printing technologies, inkjet printing, which digitally deposits ink into predetermined arrangements, is a very attractive option and has been adopted to pattern photonic components with desirable features and scales [24–30]. Moreover, the bio-friendly traits of the ink, such as biocompatibility and biodegradability, are advantageous for fabricating customized biophotonic devices.

Silk protein, which is a natural biopolymer extracted from *Bombyx mori* cocoons, is gaining much attention in biophotonic devices owing to its optical transparency [31], water-based

#389206 https://doi.org/10.1364/OME.389206
Journal © 2020 Received 24 Jan 2020; accepted 10 Feb 2020; published 26 Feb 2020

Optical Materials EXPRESS

processability [32], fabrication capabilities [33], and good preservation of functional materials [34,35], in addition to biocompatibility and biodegradability [33,36]. This unique combination of features has enabled the innovation of various silk-based biophotonic devices such as waveguides [37], photonic crystal reflectors [38], metal–insulator–metal resonators [39], distributed feedback (DFB) lasers [40], lenses [41], and surface plasmon generators [42]. In addition, solution processed silk is a promising bio-ink for the development of biosensors and responsive biophotonic devices. Recently, Parker *et al.* [43] reported a compact design for nanoscale patterned silk waveguides, and Tao *et al.* [44] introduced a cost-effective library of functional silk inks by adding organic dyes, bio-dopants, and metallic nanoparticles. Nonetheless, despite the many attractive features of silk photonics, it is still a challenge to obtain a highly coherent light source (laser) and a light coupler on the same platform using inkjet printing because the photonic devices require precise control of the device morphology in nanoscale that is challenging in the inkjet printing method. Therefore, another strategy is required to obtain the integrated form of the silk photonic components with advantages of the inkjet printing method.

Here, we report an arbitrarily patterned single-mode biolaser and a set of coupled waveguides fabricated via inkjet printing optically active functional silk ink onto a DFB board. The DFB platform consists of a 30-nm-thick titanium dioxide (TiO_2) layer deposited on a quartz grating surface. The inkjet-printed silk with rhodamine B (RhB) exhibited single-mode lasing regardless of the pattern geometry and size, down to features of diameter 200 μm. In addition, the lasing wavelength and threshold could be weakly tuned by adding gold nanoparticles (AuNPs) to the silk ink owing to the change in the effective refractive index (RI). We printed optical waveguides adjacent to the lasing part on the DFB board and observed that the edge-emitting DFB laser signal was coupled to the waveguides and propagating. Melanin nanoparticles (MNPs), which are absorptive bio-pigments, attenuated the propagating lasing signal when placed on the waveguide, thereby indicating the sensing capability of the printed optical circuit. The printed silk components were physically transient, so they could be modified by removing with water and redrawing. A suitable combination of silk protein, dopants, inkjet printing, and the DFB platform thus appears to a promising route towards on-demand integrated biophotonic circuits on a single chip for bio/chemical sensing and diagnostics.

2. Results and discussions

Figure 1(a) shows the schematic diagram for generation of photonic silk text emitting a single-mode DFB laser *via* inkjet printing. To obtain a biological light emitter, we prepared a functional bio-ink by blending silk protein solution with RhB dye (see the Methods), which is widely used in biotechnology for cell staining [45]. As the inkjet-printed layer is optically thick and has an uneven surface that inadequately induces coherent feedback of the generated light, a large DFB board (1×1 cm^2) with an ultrathin TiO_2 grating (~30-nm-thick) deposited on quartz was prepared for the arbitrarily shaped gain. Scanning electron microscopy (SEM) images show that the fabricated grating with the 380 nm pitch size (Λ) can be partially covered by the printed silk protein (Fig. 1(b)). The side-view SEM images reveal the thick and uneven layer of the printed silk (Fig. 1(c-d)). This indicates that the printed layer cannot solely support the waveguide mode to induce the long-range coherent feedback and the TiO_2-coated DFB board is important for that purpose.

Figure 2(a) shows the absorption and photoluminescence (PL) spectra of RhB in the printed silk matrix. The Λ of 380 nm was chosen for the surface emitting DFB mode to fall into the PL range of RhB, as determined by Bragg's law $\lambda_{Bragg} = \Lambda n_{eff}$, where λ_{Bragg} is the Bragg wavelength and n_{eff} is the effective RI. Under UV excitation, we could observe bright yellow light from the printed silk letters, and this light could be generated as lasing under proper excitation (Fig. 2). The inkjet-printed RhB/silk layer exhibited single-mode lasing at the wavelength of 588.3 nm (Fig. 2(b)). The second harmonic Nd:YAG laser with a wavelength of 532 nm and pulse duration

Optical Materials EXPRESS

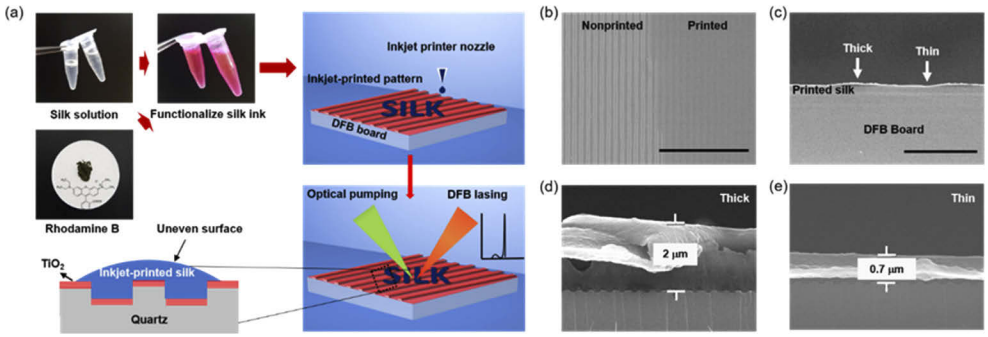

Fig. 1. Inkjet-printed silk gain on a distributed feedback (DFB) board. (a) Schematic illustration of the single mode DFB lasing from the inkjet-printed silk gain layer. Although the printed silk layer is not optically thin and uniform to support waveguide mode and DFB effect, coherent feedback can be induced by the thin TiO_2 layer on the grating. (b-e) Scanning electron microscopy (SEM) images of the printed DFB board. The top-view SEM image in b shows the clear boundary between the nonprinted and printed silk layer. The side-view SEM image in (c) shows the uneven surface of the printed silk layer. Scale bars indicate 5 μm in (b) and 50 μm in (c). Magnified SEM images are shown in (d) (at the thick layer) and (e) (at the thin layer).

of 25 ps was used for excitation and was focused on the silk layer with a 0.20 mm^2 beam spot. Where, the E-field components of the pump light source were normal to the grating surface. The single-mode lasing peak showed a full width at half maximum (FWHM) of ~2.2 nm, which is twice the minimum resolution of the spectrometer used, and red-shifted with increasing Λ (Fig. 6 in the Appendix). Far-field images (the inset of Fig. 2(b)) show that the lasing light (bottom, RhB/silk on TiO_2/quartz substrate) is much brighter than the PL (top, RhB/silk on plain quartz substrate) and can propagate along the TiO_2 layer. Figure 2(c) shows the light-in versus light-out (LL) curve to investigate the threshold behavior of the laser. We confirmed that the transition to single-mode lasing from PL happened above the input power density of 1.5 mJ/cm^2. It is worth noting that the inkjet-printed gain layer is optically too thick and uneven to induce waveguide mode for coherent feedback. In our previous study, we reported that a thin TiO_2 layer could induce coherent feedback and enhance gain even when the gain layer is not uniformly thin. Therefore, our TiO_2 coated grating platform is a good lasing canvas for the inkjet printing method, whereas typical DFB lasers require a high RI waveguide gain layer with thickness under 1 μm. Finite-difference time-domain (FDTD) simulations confirmed that the silk on the TiO_2/quartz grating supported a single DFB mode of wavelength 589.3 nm (Fig. 2(d)) and good agreement with the measured spectrum. The small difference between the simulated and experimental peaks was due to fabrication tolerance. In addition, we confirmed that the lasing wavelength increased as Λ increased in the experiments and FDTD simulations (Fig. 6 and 7 in the Appendix). At resonant wavelength, the simulation showed that photons with transverse electric (TE) polarization were strongly localized along the TiO_2 layer (Fig. 2(d)).

To investigate the minimum size of the lasing pixel, silk dots with different diameters (from 50 μm to 1600 μm) were printed on the DFB board. Lasing (population inversion) is possible when the gain enhanced by the coherent feedback exceeds the loss. This means that a large number of grooves is required to obtain sufficient feedback. DFB lasing could be observed from the printed silk dots down to features of diameter 200 μm, with lower lasing thresholds associated with larger diameters owing to the enhanced feedback (Fig. 3(a) and (b)). In addition, the reduced dot size affects the effective RI that the waveguided photons experience. FDTD simulations for the DFB grating with finite numbers of groves show that the resonant wavelength is red shifted

Optical Materials EXPRESS

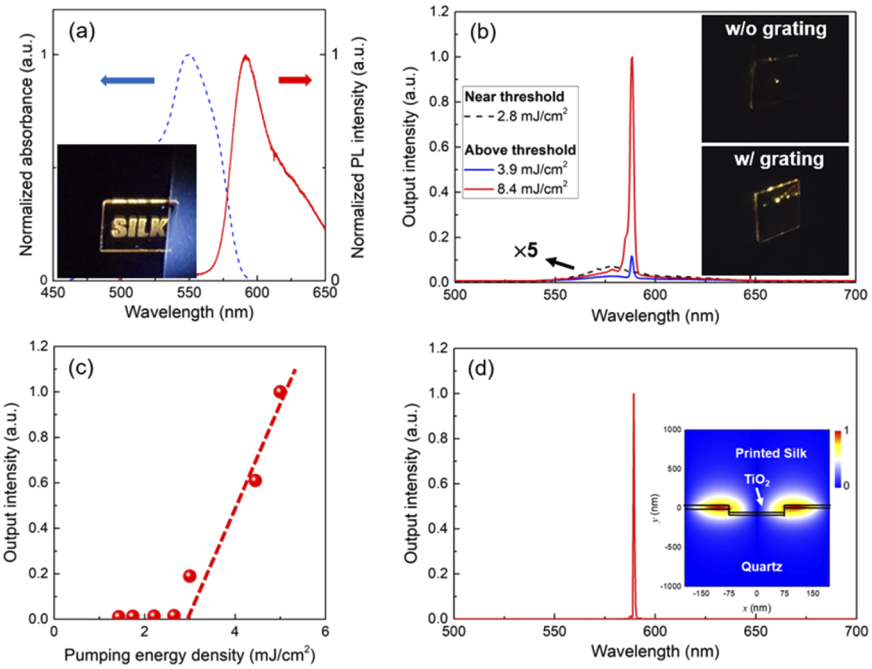

Fig. 2. Optical properties of the inkjet-printed DFB-lasing silk texts. (a) Normalized optical absorption and photoluminescence (PL) spectra of the printed silk/RhB layer. The inset shows a photograph for the printed silk text under UV laser excitation. (b) PL spectra of the printed silk/RhB letters under picosecond-pulsed excitation. Above the threshold, the lasing peak is seen at a wavelength of 588.3 nm. Insets show the photographs of the printed silk/RhB layer on the plane quartz (top) and the TiO_2-coated quartz grating (bottom). (c) Plot for the light-in *versus* light-out (LL) of the DFB laser showing threshold behavior. (d) Simulated spectrum of the DFB mode. The inset shows the electric field (parallel to the grating surface) profile of the DFB mode.

(owing to increased effective RI) and the quality factor increases (owing to increased feedback) when the number of grooves increases (Fig. 8 in the Appendix). Figure 3(a) shows that the lasing wavelength is blue shifted with decreasing dot sizes (from 591.0 nm to 583.1 nm). Over a diameter span of 1600 µm, the lasing wavelength and threshold were stabilized. These results indicate that a minimum of 1600 µm pixel is required to integrate a high-efficiency lasing source even when smaller dots can achieve lasing.

To tune the lasing wavelength, because the morphology of the grating (including Λ and height) is fixed, an additional process is required to change the RI of the silk ink. We investigated the effect of AuNP addition (biocompatible and plasmonic green absorber) on the lasing wavelength (Fig. 4(a)). Figure 4(b) shows that the lasing peak was blue shifted ($\Delta\lambda = 4.1$ nm for an AuNP-addition of 100 µl/ml) upon incorporating the AuNPs into the optical gain silk ink. The addition of AuNPs played a constructive role in reducing the effective RI of the silk film, and such a reduction of the effective RI of the gain layer could be used to tune the resonance behavior of the bio-light source to a lower wavelength [46]. Figures 9(a) and (b) (in the Appendix) show that the simulated resonance peak can be blue shifted by 4 nm when the RI of the silk superstrate is reduced to 1.52 from 1.54. Additionally, introducing a cation species into the RhB-based organic gain can also induce self-aggregation by reducing the number of excitation states. This phenomenon could be observed by the threshold behaviors of the DFB laser. Figure 4(c) shows ~2.5 times increase in threshold from 3.1 mJ/cm^2 to 7.7 mJ/mm^2 where the gain area was

Optical Materials EXPRESS

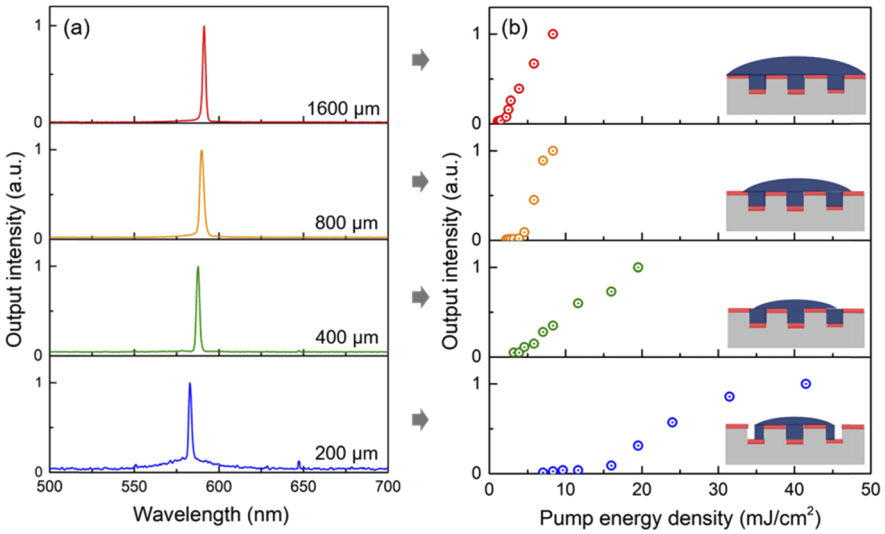

Fig. 3. Size dependence on lasing characteristics. (a) Lasing spectra with increasing diameter of the printed silk/RhB dots. (b) Corresponding LL curves to compare thresholds of lasing modes for each dot size.

occupied by the additional cation species (AuNPs) that could be explained by the blue shift in the absorption peak (Fig. 10 in the Appendix). Furthermore, no plasmonic effects were observed in the lasing spectrum (additional peaks) that could be attributed to the non-uniform surface of the printed area with a low concentration of AuNPs.

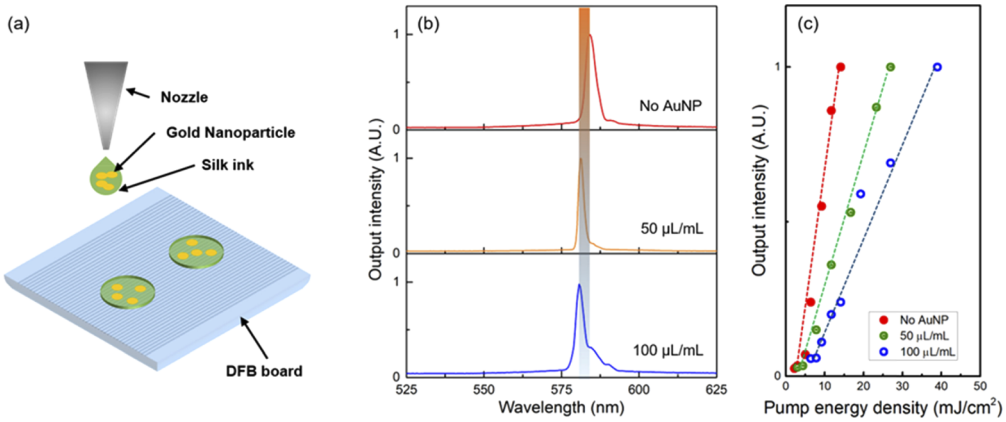

Fig. 4. Tuning of the DFB laser. (a) Schematic illustration for inkjet printing of the gold nanoparticle (AuNP) mixed silk/RhB ink. (b),(c) Lasing spectra showing the blue shift in (b) and LL plots showing threshold behaviors in (c) with increasing concentration of AuNPs.

For the integrated biophotonic circuit, we printed optical waveguides (no gain material) with a width of 200 μm near the DFB lasing region (with gain material) to couple the lasing light to the waveguides on a single DFB board with $\Lambda = 375$ nm (Fig. 5(a)). Even if the second order DFB laser used in this study shows surface emission, it contains strong edge emissions at the longer wavelength band edge of the photonic band structure [47-49] and is therefore suitable for the light source of the 2D integrated circuit. Figure 5(b) and (c) show the photographic image and

Optical Materials EXPRESS

spectra of the waveguide-coupled lasing light (lasing wavelength of 580.6 nm and threshold of 9.0 mJ/cm^2). In the edge-emitted configuration, the lasing threshold significantly increased when compared with the surface-emitted mode because of the low diffraction efficiency of the grating. In addition, the integrated platform has sensing capability to determine if the propagating light can be influenced by the analytes on the waveguide. As a proof of concept, we placed the MNP powder on the printed waveguide and observed that the waveguide-propagating laser signal was attenuated by the broadband optical absorption of the MNPs (Fig. 5(d) and (e)). The intensity of the laser light decreased by 40% when the MNP covered half the waveguide and decreased by over 90% when covering the entire waveguide. Additionally, all photonic components can be revised by *ex situ* modification (post-production modification) as the printed photonic text is physically transient. As shown in Fig. 5(f) and (g), the waveguides were partially removed by water and were reconnected by the redrawn waveguide where the coupled lasing light gathered. Inkjet printing using silk bio-ink would thus be useful for compact biophotonic devices such as lab on a chip for bio/chemical sensors and optical communication circuitry by controlling the emitted light.

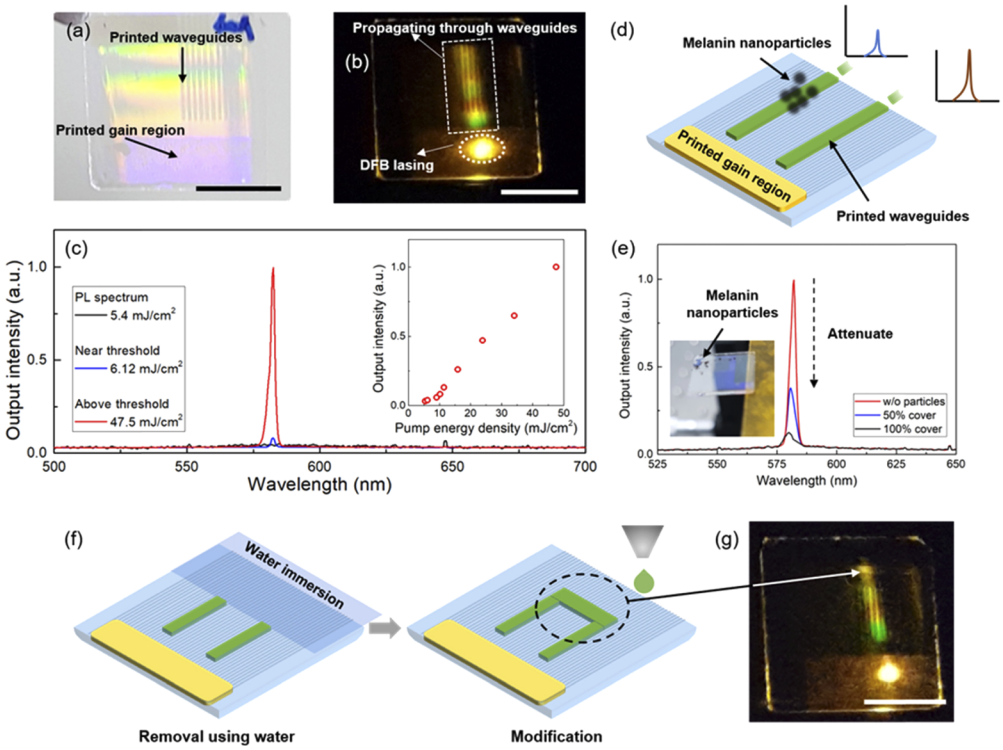

Fig. 5. Integrated biophotonic circuit printed on a DFB board (a)**,**(b) Photographs of the printed waveguide adjacent to the printed laser device (a) in daylight and (b) under pumping. The lasing light is coupled-out to the waveguide and propagated through it. (c) Measured lasing spectra at the end of the waveguide. The inset shows the LL curve of the laser. (d) Schematic illustration of the particle sensing application of the device. (e) Lasing spectra attenuated by the melanin nanoparticles on the waveguide. (f) Schematic illustration and (g) photograph for the post modification of the printed circuit by water washing and reprinting.

Optical Materials EXPRESS

3. Conclusion

We demonstrated inkjet-printed silk protein patterns that could have arbitrary shapes and show DFB lasing and waveguiding properties. Using a DFB board with a thin TiO_2 layer, the printed silk protein layer with RhB dye was able to emit single-mode DFB lasing with low threshold even though the printed layer was optically thick and nonuniform. We confirmed that the minimum diameter of the dot required to show lasing was around 200 µm. The lasing wavelength could be slightly tuned by adding nanomaterials (AuNPs in this study) to the silk ink. On the DFB board, integrated silk photonic components, including the DFB laser and coupled optical waveguides, were generated and the lasing light was coupled-out through the adjacent waveguides under excitation. On-demand modification of the printed components was possible by removal of the ink with water and redrawing. In addition, we showed the sensing capability of the printed silk photonic circuit for detecting MNPs that influenced light propagation owing to high optical absorption. Our study thus promises a new platform to utilize a photonics-based lab-on-a-chip for sensing, diagnosis, and therapy.

4. Methods

Preparation of silk ink. *Bombyx mori* cocoons were boiled in a 0.02 M Na_2CO_3 solution for 120 min to remove the sericin; the remained fibroin was rinsed with distilled water and then continuously dried in air for a day. Subsequently, the dried fibroin was dissolved in a 9.3 M LiBr solution at 60 °C for 4 h to yield a 20 wt% aqueous solution. The silk/LiBr solution was dialyzed using a dialysis membrane (Cellu-sep T1, MWCO 3.5 K, Membrane Filtration Products) at room temperature for 48 h to obtain a 6.0 wt% silk aqueous solution that was purified using a syringe filter with pore size of 0.45 µm. Furthermore, the silk solution was further diluted to 3 wt% for inkjet printing.

Rhodamine B was selected as the gain material for the inkjet-printed silk pattern. A RhB/water solution with concentration of 5×10^{-2} wt% was blended with the 3 wt% silk at the ratio 1:20 (v/v) to yield a final ratio of RhB in silk film as 0.25×10^{-3} wt%.

Fabrication of the grating. The grating template was fabricated on a square-shaped quartz substrate of size 1×1 cm^2. The 250-nm-thick layer of negative photoresist (AZ nLOF, Michrochemicals) was then spin coated on the quartz at 4000 rpm and then baked at 90 °C for 1 min. The 1D diffraction grating pattern was generated by laser interference lithography (LIL) (Fig. 11 in the Appendix). The exposure time and incident beam angle were controlled for the desired duty cycle (i.e. ~60%) and grating period, respectively. After post-exposure baking at 110 °C, the exposed resist was developed. The resist pattern was transferred to the quartz substrate using reactive ion etching equipment (RIE 80 plus, Oxford instrument). Then, a 30-nm-thick TiO_2 layer was deposited using sputter to finalize the template.

Arbitrary patterning of silk ink. One layer of the silk/RhB was inkjet printed using a Dimatix Material Printer DMP-2831 (equipped with cartridges with 21 µm nozzle diameter, FUJIFILM, Santa Clara, CA, USA) with a custom designed waveform. The droplet spacing was set as 20 µm, substrate thickness was 1000 µm, and cartridge height was 0.75 mm. The letters "SILK" and dots were printed parallel to the gratings with four nozzles at a firing voltage of around 35 V and short cleaning cycle every 45 s during the printing process.

Optical measurement. Optical measurements were performed to obtain the PL signals from the bio-light source as illustrated in Fig. 12(Please see the Appendix). The devices were pumped using the second harmonic Nd:YAG laser with a repetition rate of 10 Hz, wavelength of 532 nm, and pulse width of 25 ps. The pumping beam size (~3 mm diameter) was tightly focused onto the sample in an area of 0.20 mm^2 using a circular lens. Further, the emitted laser signal was collected by a pair of circular lenses of focal length 5 mm followed by a long pass filter to quench the role of the transmitted pump wavelength. Then, the lens collected light was fed into a 200 µm

Optical Materials EXPRESS

diameter fiber connected to an optical spectrum analyzer (USB-2000, Ocean Optics, Inc.) with a resolution of 1.2 nm. For the absorption measurement, we utilized a 1×2 fiber coupler to feed into and collect light from the sample with the optical analyzer.

Simulation. Numerical simulations were carried out by the FDTD method. 2D simulations were performed to characterize the DFB modes with the Bloch boundary condition ($k_x = 0$) along the x-direction, while the perfect matching layers were applied at the top and bottom ends in the y-direction. The cell was excited by randomly distributed multiple electric dipole sources in the silk layer. The RI of the silk was assumed as 1.54, while the RI of quartz is taken 1.48 and that TiO_2 as 2.20. Additionally, spectral and spatial data of the magnitude of the electric field was obtained by setting time conditions of 5,000 fs.

Appendix

Supplementary materials

Lasing from versatile grating periods

In order to design the inkjet-printed silk DFB lasers, it was required to analyze the operation range in terms of grating pitch size and area of the printed gain. Figure 6 shows the optical properties of the printed silk/RhB laser for gratings with different pitch sizes. Lasing peaks at wavelengths of 581, 588, and 593 nm appear on the TiO_2-coated gratings with pitch sizes of 375, 380, and 385 nm, respectively. When the pitch size is increased, the threshold also increases. FDTD simulations exhibit that the simulated resonant wavelengths are in good agreement with the measured lasing wavelengths, as shown in Fig. 7.

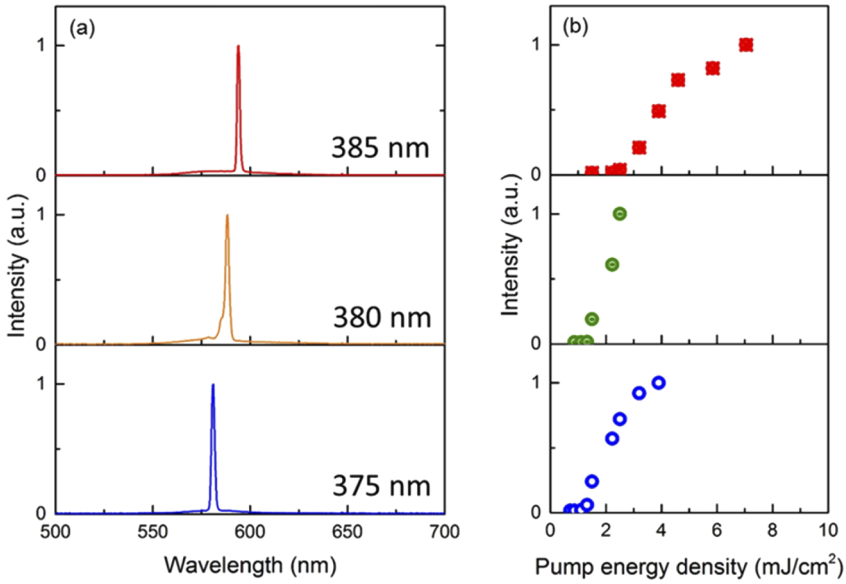

Fig. 6. DFB modes at gratings with different pitch sizes. (a) Lasing spectra from the inkjet-printed silk/RhB layer on gratings with pitch sizes of 375, 380, and 385 nm and (b) their corresponding LL curves.

Optical Materials EXPRESS

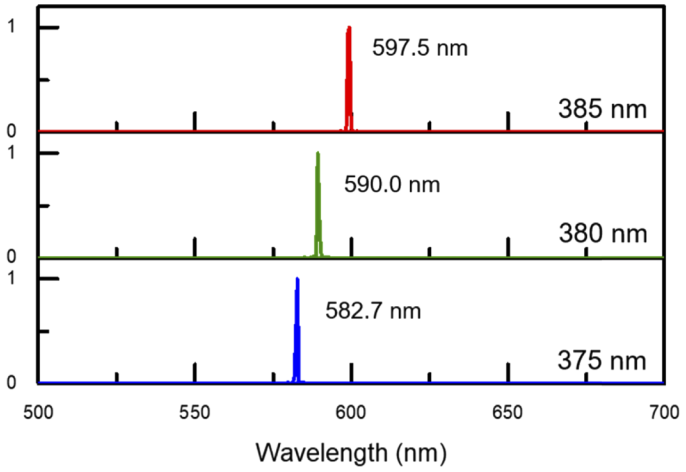

Fig. 7. Simulated spectra for DFB gratings with different pitch sizes.

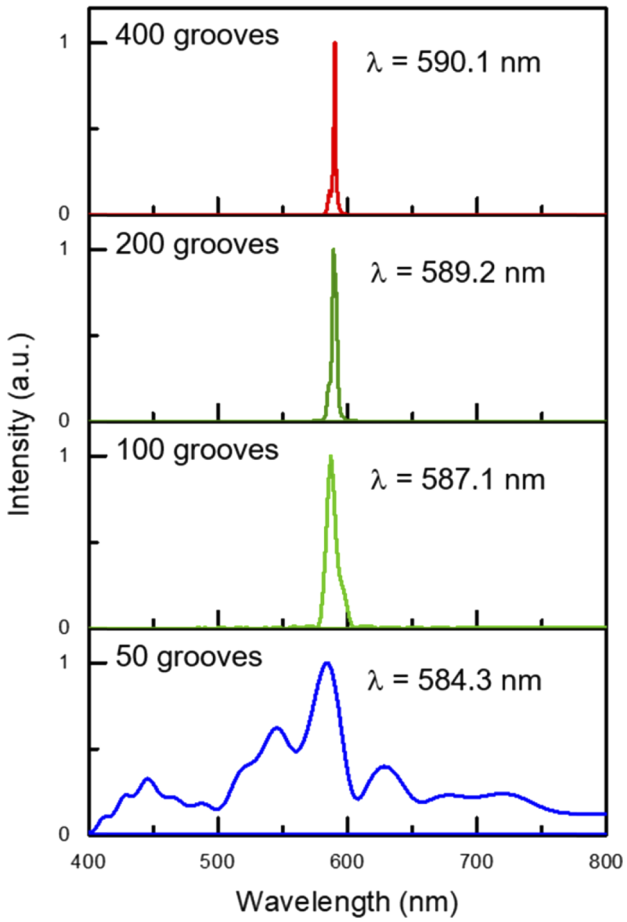

Fig. 8. Simulated spectra showing DFB resonances for gratings with different numbers of grooves. As the number of grooves increases, the resonant wavelength and quality factor also increase.

Optical Materials EXPRESS

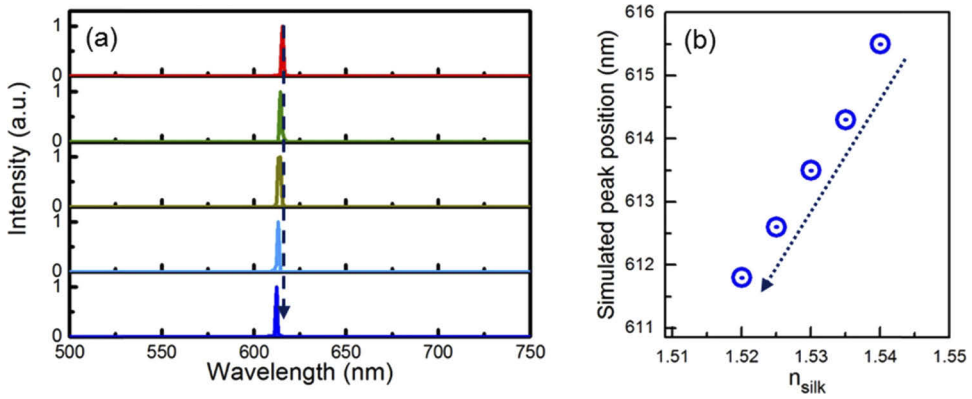

Fig. 9. Simulated spectra for the changing RI of the silk ink. (a) Simulated resonance peaks when the RI of silk is reduced by $\Delta n = 0.02$. (b) Simulated peak position by changing the RI of silk. A $\Delta\lambda$ of 4 nm is observed by reducing RI to 1.52 from 1.54.

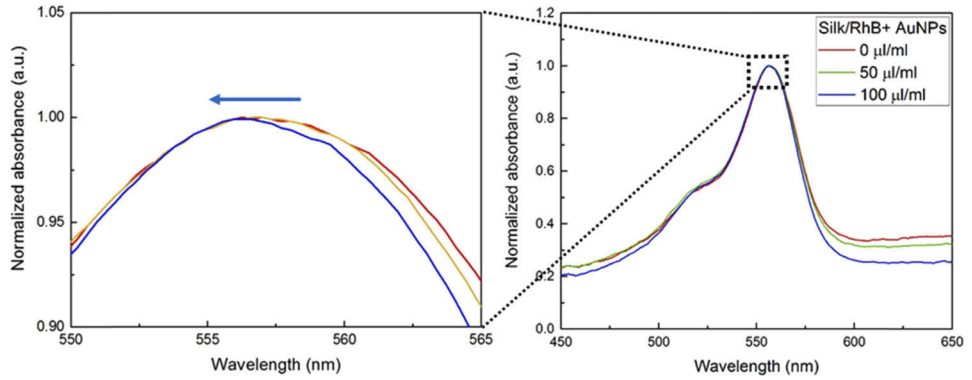

Fig. 10. Absorption spectra of silk/RhB solution containing AuNPs. Blue shift and narrowing of the absorption peak were observed after addition of AuNPs (cation species).

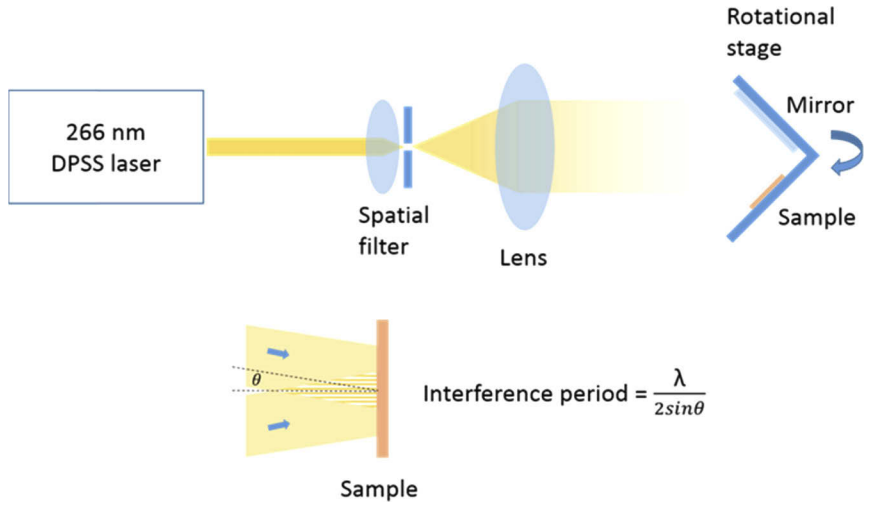

Fig. 11. Schematic illustration of the laser interference lithography process to yield second-order Bragg grating.

Optical Materials EXPRESS

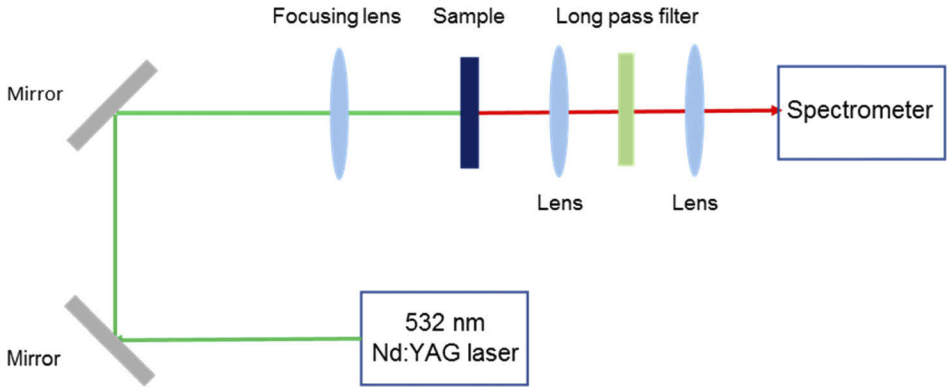

Fig. 12. Schematic illustration of pulsed laser pumping and measurement of surface emission of the inkjet-printed silk DFB laser.

Funding

LG Yonam Foundation of Korea; National Research Foundation of Korea (2018K1A3A1A39087874); Korea Institute of Energy Technology Evaluation and Planning (20184030202220); National Research Foundation of Korea (2019R1A2C2088615).

Acknowledgment

The authors acknowledge support from the LG Yonam Foundation of Korea, the National Research Foundation (NRF) of Korea (no. 2018K1A3A1A39087874 and 2019R1A2C2088615) and the Korea Institute of Energy Technology Evaluation and Planning (no. 20184030202220, Human Resources Program in Energy Technology).

Disclosures

The authors declare no competing financial interests.

References

1. S.-K. Lee, G.-R. Yi, J. H. Moon, S.-M. Yang, and D. Pine, "Pixellated photonic crystal films by selective polymerization," Adv. Mater. **18**(16), 2111–2116 (2006).
2. M. K. Choi, J. Yang, K. Kang, D. C. Kim, C. Choi, C. Park, J. S. Kim, I. S. Chae, T.-H. Kim, J. H. Kim, T. Hyeon, and D.-H. Kim, "Wearable red-green-blue quantum dot light-emitting diode array using high-resolution intaglio transfer printing," Nat. Commun. **6**(1), 7149 (2015).
3. E. O. Polat, H. B. Uzlu, O. Balci, N. Kakenove, E. Kovalska, and C. Kocabas, "Graphene-enabled optoelectronics on paper," ACS Photonics **3**(6), 964–971 (2016).
4. J. Huo, M. Li, and Y. Song, "Patterned colloidal photonic crystals," Angew. Chem., Int. Ed. **57**(10), 2544–2553 (2018).
5. D. E. Smalley, E. Nygaard, K. Squire, J. V. Wagnoer, J. Rasmussen, S. Gneiting, K. Qaderi, J. Goodsell, W. Rogers, M. Lindesy, K. Costner, A. Monk, M. Pearson, B. Haymore, and J. Peatross, "A photophoretic-trap volumetric display," Nature **553**(7689), 486–490 (2018).
6. T. Endo, M. Sato, H. Kajita, N. Okuda, S. Tanaka, and H. Hisamoto, "Printed two-dimensional photonic crystals for single-step label-free biosensing of insulin under wet conditions," Lab Chip **12**(11), 1995–1999 (2012).
7. T. Endo, C. Ueda, H. Kajita, N. Okuda, S. Tanaka, and H. Hisamoto, "Enhancement of the fluorescence intensity of DNA intercalators using nano-imprinted 2-dimensional photonic crystals," Microchim. Acta **180**(9-10), 929–934 (2013).
8. T. Yokota, P. Zalar, M. Kaltenbrunner, H. Jinno, N. Matsuhisa, H. Kitanosako, Y. Tachibana, W. Yukita, M. Koizumi, and T. Someya, "Ultraflexible organic photonic skin," Sci. Adv. **2**(4), e1501856 (2016).
9. E. Luan, H. Shoman, D. M. Ratner, K. C. Cheung, and L. Chrostowski, "Silicon photonics biosensor using label-free detection," Sensors **18**(10), 3519 (2018).
10. G. Berrettini, A. Simi, A. Malacarne, A. Bogoni, and L. Potí, "ultrafast integrable and reconfigurable XNOR, AND, NOR, and NOT photonic logic gate," IEEE Photonics Technol. Lett. **18**(8), 917–919 (2006).

Optical Materials EXPRESS

11. M. Hochberg, T. Baehr-Jones, G. Wang, M. Shearn, K. Harvard, J. Luo, Z. Chen, R. Lawson, P. Sullivan, A. K. Y. Jen, L. Dalton, and A. Scherer, "Terahertz all-optical modulation in a silicon-polymer hybrid systems," Nat. Mater. **5**(9), 703–709 (2006).
12. S. Koos, P. Vorreau, T. Vallaitis, P. Dumon, W. Bogaerts, R. Baets, B. Esembeson, I. Biaggio, T. Michinobu, F. Diederich, W. Freude, and J. Leuthold, "All-optical high-speed signal processing with silicon-organic hybrid slot waveguides," Nat. Photonics **3**(4), 216–219 (2009).
13. J. Clark and G. Lanzani, "Organic photonics for communications," Nat. Photonics **4**(7), 438–446 (2010).
14. T. Su, R. P. Scott, S. S. Djordjevic, N. K. Fontaine, D. J. Geisler, X. Cai, and S. J. B. Yoo, "Demonstration of coherent optical communication using integrated silicon photonic orbital angular momentum devices," Opt. Express **20**(9), 9396–9402 (2012).
15. C.-A. Fustin, G. Glasser, H. W. Spiess, and U. Jonas, "Site-selective growth of colloidal crystals with photonic properties on chemically patterned surfaces," Adv. Mater. **15**(12), 1025–1028 (2003).
16. E. Ozbay, "Plasmonics: merging photonics and electronics at nanoscale dimensions," Science **311**(5758), 189–193 (2006).
17. Z. Wang, J. Zhang, J. Xie, Y. Yin, Z. Wang, H. Shen, Y. Li, J. Li, S. Liang, L. Cui, L. Zhang, H. Zhang, and B. Yang, "Patterning organic/inorganic hybrid bragg stacks by integrating one-dimensional photonic crystals and microcavities through photolithography: towards tunable colorful patterns as highly selective sensors," Appl. Mater. Interfaces **4**(3), 1397–1403 (2012).
18. J. S. King, E. Graugnard, O. M. Roche, D. N. Sharp, J. Scrimgeour, R. G. Denning, A. J. Turberfield, and C. J. Summers, "Infiltration and inversion of holographically defined polymer photonic crystal templates by atomic layer deposition," Adv. Mater. **18**(12), 1561–1565 (2006).
19. C. Glynn and C. O'Dwyer, "Solution processable metal oxide thin film deposition and material growth for electronics and photonics devices," Adv. Mater. Interfaces **4**(2), 1600610 (2017).
20. S. Arif, M. Umar, and S. Kim, "Interacting metal-insulator-metal resonator by nanaoporous silver and silk protein nanomembranes and its water-sensing applications," ACS Omega **4**(5), 9010–9016 (2019).
21. Y. A. Vlasov, X.-Z. Bo, J. C. Sturm, and D. J. Norris, "On-chip natural assembly of silicon photonic bandgap crystals," Nature **414**(6862), 289–293 (2001).
22. T. F. Krauss, "Planar photonic crystal waveguide devices for integrated optics," Phys. Stat. Sol. (a) **197**(3), 688–702 (2003).
23. H. Jung, K. Min, H. Jeon, and S. Kim, "Physically transient distributed feedback laser using optically activated silk bio-ink," Adv. Opt. Mater. **4**(11), 1738–1743 (2016).
24. L. Cui, Y. Li, J. Wang, E. Tian, X. Zhang, Y. Zhang, Y. Song, and L. Jiang, "Fabrication of large-area patterned photonic crystals by ink-jet printing," J. Mater. Chem. **19**(31), 5499–5502 (2009).
25. J. Wang, L. Wang, Y. Song, and L. Jiang, "Patterned photonic crystals fabricated by inkjet printing," J. Mater. Chem. C **1**(38), 6048–6058 (2013).
26. M. Kuang, J. Wang, B. Bao, F. Li, L. Wang, L. Jiang, and Y. Song, "Inkjet printing pattered photonic crystal demos for wide viewing-angle displays by controlling the sliding three phases contact line," Adv. Opt. Mater. **2**(1), 34–38 (2014).
27. T. Wolfer, P. Bollgruen, D. Mager, L. Overmeyer, and J. G. Korvink, "Flexographic and inkjet printing of polymer optical waveguides for fully integrated sensor systems," Proc. Technol. **15**, 521–529 (2014).
28. A. Samusjew, M. Kratzer, A. Moser, C. Teichert, K. K. Krawczyk, and T. Griesser, "Inkjet printing of soft, stretchable optical waveguides through the photopolymerization of high-profile linear patterns," ACS Appl. Mater. Interfaces **9**(5), 4941–4947 (2017).
29. Y.-M. Liao, W.-C. Liao, S.-W. Chang, C.-F. Hou, C.-T. Tai, C.-Y. Su, Y.-T. Hsu, M.-H. Wu, R.-J. Chou, Y.-H. Lee, S.-Y. Lin, W.-J. Lin, C.-H. Chang, G. Haider, M. Kataria, P. K. Roy, K. P. Bera, C. R. Paullnbaraj, H.-W. Hu, T.-Y. Lin, and Y.-F. Chen, "Inkjet-printed random lasers," Adv. Mater. Technol. **3**(12), 1800214 (2018).
30. F. Mathies, P. Brenner, G. Hernandez-Sosa, I. A. Howard, U. W. Paetzold, and U. Lemmer, "Inkjet-Printed Perovskite distributed feedback lasers," Opt. Express **26**(2), A144–A152 (2018).
31. K. Min, M. Umar, S. Ryu, S. Lee, and S. Kim, "Silk protein as a new optically transparent adhesion layer for an ultra-smooth sub-10 nm gold layer," Nanotechnology **28**(11), 115201 (2017).
32. S. Kim, B. Marelli, M. A. Brenckle, A. N. Mitropoulos, E.-S. Gil, K. Tsioris, H. Tao, D. L. Kaplan, and F. G. Omenetto, "All-water-based electron-beam lithography using silk as a resist," Nat. Nanotechnol. **9**(4), 306–310 (2014).
33. F. G. Omenetto and D. L. Kaplan, "A new route for silk," Nat. Photonics **2**(11), 641–643 (2008).
34. Y. Choi, H. Jeon, and S. Kim, "A fully biocompatible single-mode distributed feedback laser," Lab Chip **15**(3), 642–645 (2015).
35. I. B. Dogru, K. Min, M. Umar, H. B. Jalali, E. Begar, D. Conkar, E. N. F. Karalar, S. Kim, and S. Nizamoglu, "Single transverse mode protein laser," Appl. Phys. Lett. **111**(23), 231103 (2017).
36. W. Huang, S. Ling, C. Li, F. G. Omenetto, and D. L. Kaplan, "Silkworm silk-based materials and devices generated using bio-nanotechnology," Chem. Soc. Rev. **47**(17), 6486–6504 (2018).
37. V. Prajzler, K. Min, S. Kim, and P. Nekvindova, "The investigation of the waveguiding properties of silk fibroin from the visible to near-infrared spectrum," Materials **11**(1), 112 (2018).

Optical Materials EXPRESS

38. K. Min, S. Kim, and S. Kim, "Deformable and conformal silk hydrogel inverse opal," Proc. Natl. Acad. Sci. U. S. A. **114**(24), 6185–6190 (2017).
39. H. Kwon and S. Kim, "Chemically tunable, biocompatible, and cost-effective metal–insulator–metal resonators using silk protein and ultrathin silver films," ACS Photonics **2**(12), 1675–1680 (2015).
40. M. Umar, K. Min, and S. Kim, "A physically transient and eco-friendly distributed feedback laser chemosensor for detecting acid vapor," Sens. Actuators, B **255**(3), 3207–3215 (2018).
41. H. Tao, J. M. Kainerstorfer, S. M. Siebert, E. M. Pritchard, A. Sassaroli, B. J. B. Panilaitis, M. A. Brenckle, J. J. Amsden, J. Levitt, S. Fantini, D. L. Kaplan, and F. G. Omenetto, "Implantable, multifunctional, bioresorbable optics," Proc. Natl. Acad. Sci. U. S. A. **109**(48), 19584–19589 (2012).
42. M. Lee, H. Jeon, and S. Kim, "A highly tunable and fully biocompatible silk nanoplasmonic optical sensor," Nano Lett. **15**(5), 3358–3363 (2015).
43. S. T. Parker, P. Domachuk, J. Amsden, J. Bressner, J. A. Lewis, D. L. Kaplan, and F. G. Omenetto, "Biocompatible silk printed optical waveguides," Adv. Mater. **21**(23), 2411–2415 (2009).
44. H. Tao, B. Marelli, M. Yang, B. An, M. S. Onses, J. A. Rogers, D. L. Kaplan, and F. G. Omenetto, "Inkjet printing of regenerated silk fibroin: from printable forms to printable functions," Adv. Mater. **27**(29), 4273–4279 (2015).
45. K. Aslan, I. Gryczynski, J. Malicka, E. Matveeva, J. R. Lakowicz, and C. D. Geddes, "Metal-enhanced fluoresence: An emerging tool in biotechnology," Curr. Opin. Biotechnol. **16**(1), 55–62 (2005).
46. R. R. Da Silva, C. T. Dominguez, M. V. dos Santos, R. Barbosa-Silva, M. Cavicchioli, L. M. Christovan, L. S. A. de Melo, A. S. L. Gomes, C. B. de Araújo, and S. J. L. Ribeiro, "Silk fibroin biopolymer films as efficient hosts for dfb laser operation," J. Mater. Chem. C **1**(43), 7181–7190 (2013).
47. P. J. Dowling, M. Scalora, M. J. Bloemer, and C. M. Bowden, "The photonic band edge laser: A new approach to gain enhancement," J. Appl. Phys. **75**(4), 1896–1899 (1994).
48. M. Nagawa, M. Ichikawa, T. Koyama, H. Shirai, and Y. Taniguchi, "Organic Solid-State Distributed Feedback dye Laser with a Nonmorphological Modification Grating," Appl. Phys. Lett. **77**(17), 2641–2643 (2000).
49. G. A. Turnbull, P. Andrew, M. J. Jory, W. L. Barnes, and I. D. W. Samuel, "Relationship Between Photonic Band Structure and Emission Characteristics of a Polymer Distributed Feedback Laser," Phys. Rev. B **64**(12), 125122 (2001).